

# Chemical pressure effect on the optical conductivity of the nodal-line semimetals ZrSiY ( $Y=S, \text{Se}, \text{Te}$ ) and ZrGeY ( $Y=S, \text{Te}$ )

J. Ebad-Allah,<sup>1,2</sup> J. Fernández Afonso,<sup>3</sup> M. Krottenmüller,<sup>1</sup> J. Hu,<sup>4</sup>  
Y. L. Zhu,<sup>5,6</sup> Z. Mao,<sup>5,6</sup> J. Kuneš,<sup>3,7,\*</sup> and C. A. Kuntscher<sup>1,†</sup>

<sup>1</sup>*Experimentalphysik II, Augsburg University, 86159 Augsburg, Germany*

<sup>2</sup>*Department of Physics, Tanta University, 31527 Tanta, Egypt*

<sup>3</sup>*Institute of Solid State Physics, TU Wien, 1020 Vienna, Austria*

<sup>4</sup>*Department of Physics, University of Arkansas, Fayetteville, AR 72701, USA*

<sup>5</sup>*Department of Physics, Pennsylvania State University, University Park, PA 16803, USA*

<sup>6</sup>*Department of Physics and Engineering Physics,  
Tulane University, New Orleans, LA 70118, USA*

<sup>7</sup>*Institute of Physics, The Czech Academy of Sciences, 18221 Praha, Czech Republic*

ZrSiS is a nodal-line semimetal, whose electronic band structure contains a diamond-shaped line of Dirac nodes. We carried out a comparative study on the optical conductivity of ZrSiS and related compounds ZrSiSe, ZrSiTe, ZrGeS, and ZrGeTe by reflectivity measurements over a broad frequency range combined with density functional theory calculations. The optical conductivity exhibits a distinct U-shape, ending at a sharp peak at around  $10000 \text{ cm}^{-1}$  for all studied compounds, except for ZrSiTe. The U-shape of the optical conductivity is due to transitions between the linearly dispersing bands crossing each other along the nodal line. The sharp high-energy peak is related to transitions between almost parallel bands, and its energy position depends on the interlayer bonding correlated with the  $c/a$  ratio, which can be tuned by either chemical or external pressure. For ZrSiTe, another pair of crossing bands appears in the vicinity of the Fermi level, corrugating the nodal-line electronic structure and leading to the observed difference in optical conductivity. The findings suggest that the Dirac physics in ZrXY compounds with  $X=\text{Si}, \text{Ge}$  and  $Y=\text{S}, \text{Se}, \text{Te}$  is closely connected to the interlayer bonding.

## I. INTRODUCTION

The quest for novel topological materials with exceptional properties has led in recent years to an enormous research activity on two-dimensional (2D) and three-dimensional (3D) Dirac semimetals hosting massless Dirac fermions. In Dirac semimetals linearly dispersing bands cross at isolated points at the Fermi energy  $E_F$ , resulting in a dispersion locally resembling that of massless fermions. The most popular example for a 2D Dirac semimetal is graphene exhibiting highly interesting properties like outstanding mechanical stability [1], ultrahigh electron mobility [2], and superior thermal conductivity [3]. In contrast to Dirac semimetals with discrete Dirac points or nodes, in nodal-line semimetals the linearly dispersing bands cross along a line in the Brillouin zone. Corrugation of the nodal lines in the energy direction then gives rise to rod shaped Fermi surfaces, which are sensitive to small changes of external parameters.

ZrSiS is a nodal-line semimetal with a diamond-rod-shaped Fermi surface resulting from an almost ideal nodal-line band structure. It was suggested that its band structure contains additional Dirac-like band crossings located several hundred meV above below  $E_F$ , which are protected by non-symmorphic symmetry [4–6]. ZrSiS is exceptional among the Dirac materials since the linearly

dispersing bands at  $E_F$  extend over a rather large energy range of up to 2 eV, although spin-orbit coupling introduces a small gap ( $\sim 0.02 \text{ eV}$ ) to the Dirac nodes. It shows exceptional properties like unusual magnetoresistance characteristics [7, 8], high mobility of charge carriers [8, 9] and correlation effects [10], which renders ZrSiS a highly interesting material.

ZrSiS belongs to the family of compounds ZrXY, where  $X$  can be a carbon group element ( $X=\text{Si}, \text{Ge}, \text{Sn}$ ) and  $Y$  is a chalcogen element ( $Y=\text{S}, \text{Se}, \text{Te}$ ) [11]. In this compound family the 2D-to-3D structural dimensionality evolution induced by isoelectronic substitution, which is generally called chemical pressure, was suggested to be realized and to be monitored *via* the ratio of lattice parameters  $c/a$  [11, 12]. This renders ZrXY a model system to probe the effect of structural dimensionality change on nodal-line semimetals.

Earlier optical studies on ZrSiS found a rather flat optical conductivity in the energy range 30 – 300 meV, which was claimed to be due to 2D Dirac bands near  $E_F$  [13]. This interpretation was, however, questioned recently by theoretical calculations [14]. The high-energy optical conductivity exhibits a distinct U-shape ending at a sharp kink/peak around  $10000 \text{ cm}^{-1}$ , which was not addressed previously [13].

We present a combined experiment+theory study of several members of the ZrXY family, which addresses these features and relate them to the nodal-line electronic structure of the materials. In particular, we find that ZrSiS, ZrSiSe, ZrGeS, and ZrGeTe have very close to ideal nodal-line band structure with varying degree

\* kunes@ifp.tuwien.ac.at

† christine.kuntscher@physik.uni-augsburg.de

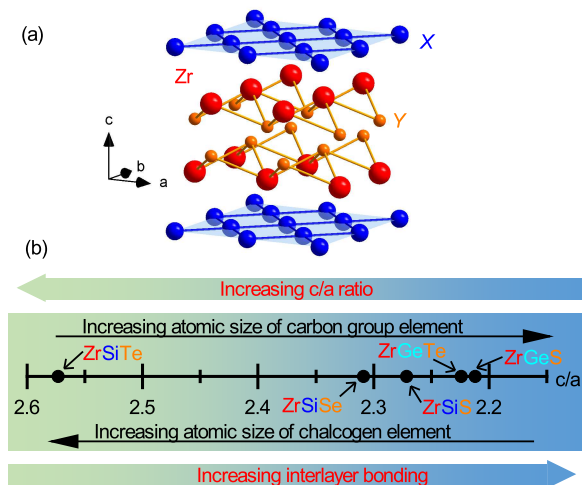


FIG. 1. (a) Crystal structure of the  $\text{ZrXY}$  compounds with square nets parallel to the  $ab$  plane. (b) Scheme illustrating the chemical pressure effect in  $\text{ZrSiS}$ ,  $\text{ZrSiSe}$ ,  $\text{ZrSiTe}$ ,  $\text{ZrGeS}$ , and  $\text{ZrGeTe}$ .

of corrugation of the nodal line, while in  $\text{ZrSiTe}$  another pair of crossing bands appears in the vicinity of the Fermi level, destroying the nodal-line structure and pushing it away from  $E_F$  in parts of the Brillouin zone.

The compounds  $\text{ZrXY}$  crystallize in a  $\text{PbFCl}$ -type structure in the tetragonal  $\text{P4/nmm}$  space group with non-symmorphic symmetry [see Fig. 1(a)] [11]. The layered crystal structure contains square nets of  $X$  atoms parallel to the  $ab$  plane, where each  $X$  square net is sandwiched between two  $\text{Zr}$  square nets. Each  $X$  atom has bonding to four  $\text{Zr}$  atoms in tetrahedral coordination. The chalcogen atoms  $Y$  also form square nets in the  $ab$  plane. Hence, the crystal structure of  $\text{ZrXY}$  consists of slabs with five square nets with a stacking sequence  $[\text{Y-Zr-X-Zr-Y}]$ , terminated by  $Y$  square nets on both sides [8]. The bonding between two adjacent slabs is of van der Waals type and hence weak. Therefore, these crystals generally tend to cleave along the plane between two chalcogen layers.

It was proposed that the structural dimensionality of the  $\text{ZrXY}$  materials can be tuned by chemical pressure, i.e., isoelectronic substitution, and monitored *via* the ratio of lattice parameters  $c/a$ , where  $c$  is the distance between two adjacent  $\text{Si}$  square nets and  $a$  is the in-plane lattice parameter of the tetragonal crystal structure [11, 12]. The  $c/a$  ratio may serve as a measure for the interlayer bonding strength in the system. As illustrated in Fig. 1(b), the chemical pressure effect in the studied  $\text{ZrXY}$  compounds can be realized either by the isoelectronic substitution of the carbon group element  $X$  or the chalcogen element  $Y$ . With increasing the atomic size of the chalcogen element  $Y$  the slab thickness along the  $c$  axis increases and hence the  $c/a$  ratio increases, causing a decrease in the interlayer bonding. Accordingly, the chemical pressure in  $\text{ZrSiTe}$  is reduced as compared

to  $\text{ZrSiS}$ , and therefore  $\text{ZrSiTe}$  was described as a layered material without significant interlayer bonding [11]. In contrast, with increasing atomic size of the carbon group element  $X$  the  $c/a$  ratio decreases, and thus tunes the interlayer bonding in the opposite way. For example, in  $\text{ZrSiS}$  a smaller interlayer bonding is expected as compared to  $\text{ZrGeS}$  [see Fig. 1(b)]. In the case of the  $X$  substitution, the chemical pressure effect is, however, less direct as described in Ref. 11: The increasing atomic size of  $X$  leads to longer  $X$ - $X$  bonds within the  $X$  square nets, which affects the in-plane  $Y$ - $Y$  spacing as well. The cell parameter  $c$  is decreased, while the unit cell expands along the  $a$  direction. The net effect is an enhancement of the interlayer bonding in adjacent  $[\text{Y-Zr-X-Zr-Y}]$  slabs.

Among all studied materials,  $\text{ZrSiTe}$  has the highest  $c/a$  ratio, with a value close to 2.6, and therefore supposedly has a smaller interlayer bonding. This is confirmed by de Haas-van Alphen quantum oscillation measurements, which show that the Fermi surface has a 2D character in  $\text{ZrSiTe}$ , in contrast to  $\text{ZrSiS}$  and  $\text{ZrSiSe}$  ( $c/a$  ratio close to 2.3) with a 3D-like Fermi surface [15]. This also explains why  $\text{ZrSiTe}$  single crystals can be easily exfoliated mechanically.

## II. SAMPLE PREPARATION, EXPERIMENTAL AND COMPUTATIONAL DETAILS

Single crystals  $\text{ZrSiY}$  ( $Y=\text{S, Se, Te}$ ) and  $\text{ZrGeY}$  ( $Y=\text{S, Te}$ ) were grown by a chemical vapor transport method [9, 16]. The samples were characterized by x-ray diffraction and energy-dispersive x-ray spectroscopy, in order to ensure phase-purity and crystal quality.

The reflectivity measurements were carried out in the frequency range ( $\approx 100 - 24000 \text{ cm}^{-1}$ ) with an infrared microscope (Bruker Hyperion), equipped with a  $15\times$  Cassegrain objective, coupled to a Bruker Vertex v80 Fourier transform infrared spectrometer. Reflectivity measurements on  $\text{ZrSiSe}$ ,  $\text{ZrSiTe}$ , and  $\text{ZrGeTe}$  were performed on freshly cleaved (001) surfaces. Since  $\text{ZrSiS}$  and  $\text{ZrGeS}$  crystals cannot be easily cleaved, the as-grown, shiny (001) surfaces were carefully cleaned with isopropanol before the reflectivity measurements. The reproducibility of the results was checked on several crystals for each compound. To obtain the absolute reflectivity spectra, the intensity reflected from an Al mirror served as reference. The reflectivity measurements were carried out at room temperature, since the dependence of the optical response on temperature is relatively weak, especially regarding the interband transitions, as was shown for  $\text{ZrSiS}$  [13].

The frequency-dependent dielectric function  $\epsilon(\omega)$  and optical conductivity  $\sigma(\omega)$  of the materials were obtained via Kramers-Kronig analysis of the reflectivity spectra. To this end, the reflectivity data were extrapolated to low frequencies based on the Drude-Lorentz fitting, while x-ray atomic scattering functions [17] were used for calculating the higher-frequency extrapolations. A power law

$1/\omega^n$  with  $n$  up to 3 was used for interpolating the reflectivity spectra between the measured and calculated data. The contributions to the optical conductivity spectra  $\sigma_1$  were obtained by simultaneous Drude-Lorentz fitting of the reflectivity and optical conductivity.

Pressure-dependent reflectance measurements up to 3.5 GPa at room temperature were carried out with an infrared microscope (Bruker Hyperion) coupled to a Bruker Vertex v80 Fourier transform infrared spectrometer in the frequency range 600-23000  $\text{cm}^{-1}$ . All the pressure-dependent reflectivity spectra refer to the absolute reflectivity at the sample-diamond interface, denoted as  $R_{\text{sd}}$ . The reflectivity spectrum  $R_{\text{sd}}(\omega)$  was calculated according to  $R_{\text{sd}}(\omega) = R_{\text{dia}} \times I_s(\omega)/I_{\text{ref}}(\omega)$ , where  $I_s$  is the intensity of the radiation reflected from the sample-diamond interface,  $I_{\text{ref}}$  is the intensity reflected from the inner diamond-air interface of the empty diamond anvil cell, and  $R_{\text{dia}} = 0.167$ , which is assumed to be pressure independent [18].

The pressure-dependent reflectivity spectra are affected in the frequency range between 1800 and 2670  $\text{cm}^{-1}$  by multi-phonon absorptions in the diamond anvils, which are not completely corrected by the normalization procedure. Therefore, this part of the spectrum was interpolated based on the Drude-Lorentz fitting. The measured reflectivity data were extrapolated to low frequencies based on Drude-Lorentz fit for further analysis. For the high-frequency extrapolation the simulated free-standing reflectivity spectrum (see above) was used, taking into account the sample-diamond interface. The real part of the optical conductivity  $\sigma_1$  was obtained via Kramers Kronig transformation of the reflectivity spectrum [19].

Density functional theory (DFT) calculations have been performed using the Wien2k [20] code. The calculations were carried out with the Generalized Gradient Approximation as exchange correlation functional, 1000 k-points in the self-consistent calculation and 200000 k-point to evaluate the optical conductivity.

In order to gain insight into the origin of the studied band structures we have constructed a tight-binding model in the basis of Zr- $d$ , Si- $s, p$  and Y- $p$  Wannier functions. To this end we have used wannier90 [21] and wien2wannier [22] packages.

### III. RESULTS

The real part of the optical conductivity  $\sigma_1(\omega)$  of ZrSiS [see Fig. 2 and suppl. Fig. S2(a)] contains two Drude contributions at low energies stemming from electron-type and hole-type itinerant charge carriers, consistent with the recently reported findings of an extremely large magnetoresistance [7, 23]. Besides the Drude contributions, the low-energy optical conductivity shows a plateau-like behavior in the range  $\sim 240 - 2400 \text{ cm}^{-1}$ , which was claimed to be due to 2D Dirac bands near  $E_F$  [13]. In analogy to graphene, in a 2D system with an ideal linear

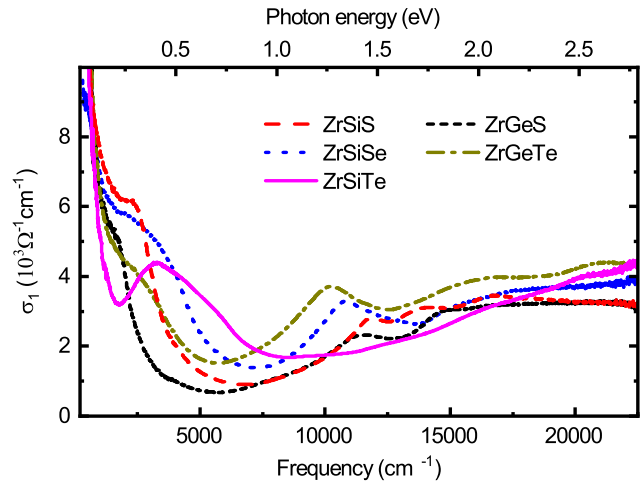


FIG. 2. Experimental optical conductivity spectra for all measured ZrXY compounds as obtained from ambient-condition reflectivity spectra.

dispersion of Dirac bands one would expect a constant optical conductivity [24–26]. The interpretation of the flat conductivity in ZrSiS in terms of 2D Dirac bands was, however, questioned recently by theoretical calculations [14]. The drop in the optical conductivity for higher frequencies and the subsequent rise result in a broad dip centered at 6700  $\text{cm}^{-1}$ , i.e., a U-shaped optical conductivity [see Figs. 2 and 3(a)]. The high-energy optical conductivity of ZrSiS is rather flat, overlayed with three well-resolved absorption features, which have not been considered previously. Among them, the sharp peak at 11650  $\text{cm}^{-1}$  [labelled L4 in Fig. 3(b)] is the most pronounced. A similar profile of the optical conductivity spectrum – namely a distinct U-shape ending at a sharp peak – is found for the materials ZrSiSe, ZrGeS, and ZrGeTe (see Figs. 2 and 3). In particular, the high-energy L4 peak is present in all three compounds with slight variation in its energy position depending on the carbon group element and the chalcogen element (chemical pressure).

In comparison to the other studied ZrXY materials, the optical conductivity profile of ZrSiTe is distinctly different [see Figs. 2 and 3(d)]. Besides the Drude-like characteristics, the low-energy range is dominated by a pronounced absorption band centered at  $\approx 3300 \text{ cm}^{-1}$  with a shoulder on its high-frequency side [see suppl. Fig. S2(c)]. Above 9000  $\text{cm}^{-1}$  the optical conductivity monotonically increases with increasing frequency without any well-resolvable feature. Most importantly, the sharp peak at around 10.000  $\text{cm}^{-1}$  is no longer present in ZrSiTe.

#### A. Theoretical optical spectra

In order to understand the measured optical conductivities we have performed density functional calculations with Wien2k [20] code for obtaining the electronic band

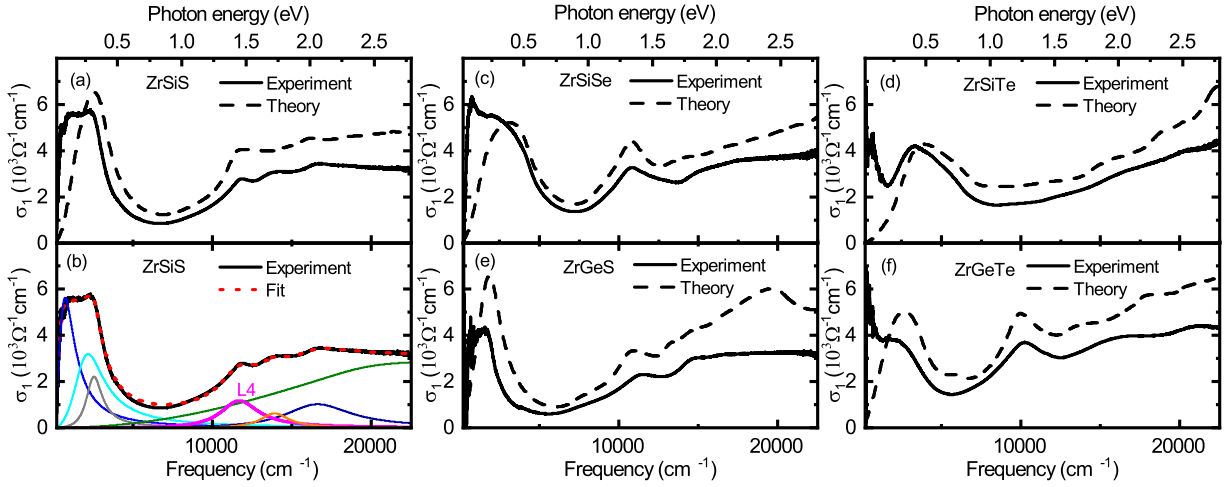


FIG. 3. (a), (c)-(f): Comparison of the experimental and theoretical optical conductivity without intraband contributions for ZrSiS, ZrSiSe, ZrSiTe, ZrGeS, and ZrGeTe, respectively. (b) Contributions to the experimental optical conductivity of ZrSiS as obtained from the fitting are shown, in particular the sharp peak labelled L4, which is due to transitions between almost parallel bands.

structure and optical spectra. Here, we focus on the high-energy features in the optical spectra  $> 3000 \text{ cm}^{-1}$  and thus we did not consider the Drude intra-band contributions. The spin-orbit coupling plays no role in the optical conductivity in this frequency range. Starting from the scalar-relativistic (no spin-orbit coupling) band structure, the spin-orbit coupling opens or enhances a small gap between the crossing bands forming the nodal line in the vicinity of the Fermi level. It thus affects the  $dc$  transport and low-energy optical conductivity, however, being restricted to a low-dimensional subspace (vicinity of the nodal-line) of the Brillouin zone, the spin-orbit splitting was found to have no discernible effect on the optical conductivity in the frequency range  $> 3000 \text{ cm}^{-1}$ .

The comparison in Fig. 3 reveals a good quantitative agreement between experiment and theory for all studied compounds. With ZrSiTe being a clear outlier, all the remaining compounds exhibit a U-shaped optical conductivity between  $3000\text{-}10000 \text{ cm}^{-1}$ , bounded on the low-energy side by a flat region and on the high-energy side by a sharp peak (see Fig. 3). In order to understand the origin of these features, we show the calculated band structure together with a decomposition of the optical conductivity and joint density of states (JDOS) into contributions of different band combinations in Fig. 4. We point out that this decomposition is merely an analytic tool and does not have a deeper physical meaning.

First, we discuss the spectrum of ZrSiS. The dropping side of the U-shaped region of the optical conductivity spectrum ( $< 6000 \text{ cm}^{-1}$ ) is dominated by the transitions between the linear crossing bands close to  $E_F$ , marked green and yellow in Fig. 4(a). The rising side of the U-shaped region is due to other band combinations. Analyzing the band and k-point contribution to the optical conductivity, the sharp L4 kink marking the upper bound of the U-shaped region can be assigned to transi-

tions between the almost parallel red and yellow bands in the vicinity of the  $X$  and  $R$  points, as marked in Fig. 4(a). This interpretation was first pointed out by Habe and Koshino [14]. Therefore, the position of the kink in all the studied materials, except for ZrSiTe, follows the red/yellow splitting at the  $X$  and  $R$  points.

The comparison of the optical conductivity in Fig. 4(b) with the JDOS in Fig. 4(c) reveals a strong k- and/or frequency dependence of the dipole matrix elements. This makes the theoretical studies assuming constant matrix elements [24, 26] of limited use for the present material. Nevertheless, it is instructive to discuss the JDOS of the lowest bands, which exhibits a broad constant region following the initial onset [black line in Fig. 4(c)]. This JDOS shape reflects the relative dispersion of the valence (green) and conduction (yellow) bands, which is linear in one direction and almost constant in the remaining two. Such a 1D linear dispersion gives rise to a constant JDOS (as well as to a constant density of states). The onset region reflects the deviation from this idealization due to corrugation of the nodal line and gap opening in the bulk of the Brillouin zone. We observe numerically that in all the studied materials the low-frequency limit of the U-shaped region correlates with the boundary of the constant JDOS. Our analysis thus contrasts the interpretation of Ref. [13], which ascribed the spectra between  $250\text{-}2500 \text{ cm}^{-1}$  to the linear bands and estimated the deviations from the nodal-line shape due to gap opening or shift away from the Fermi level to 30 meV. Our numerical results suggest the deviations from the perfect nodal-line structure to be an order of magnitude bigger, largely due to corrugation of the nodal line (shift away from the Fermi level).

To summarize, the U-shape of the optical conductivity reflects the proximity an idealized band structure with two linearly crossing (touching) bands along a surface in



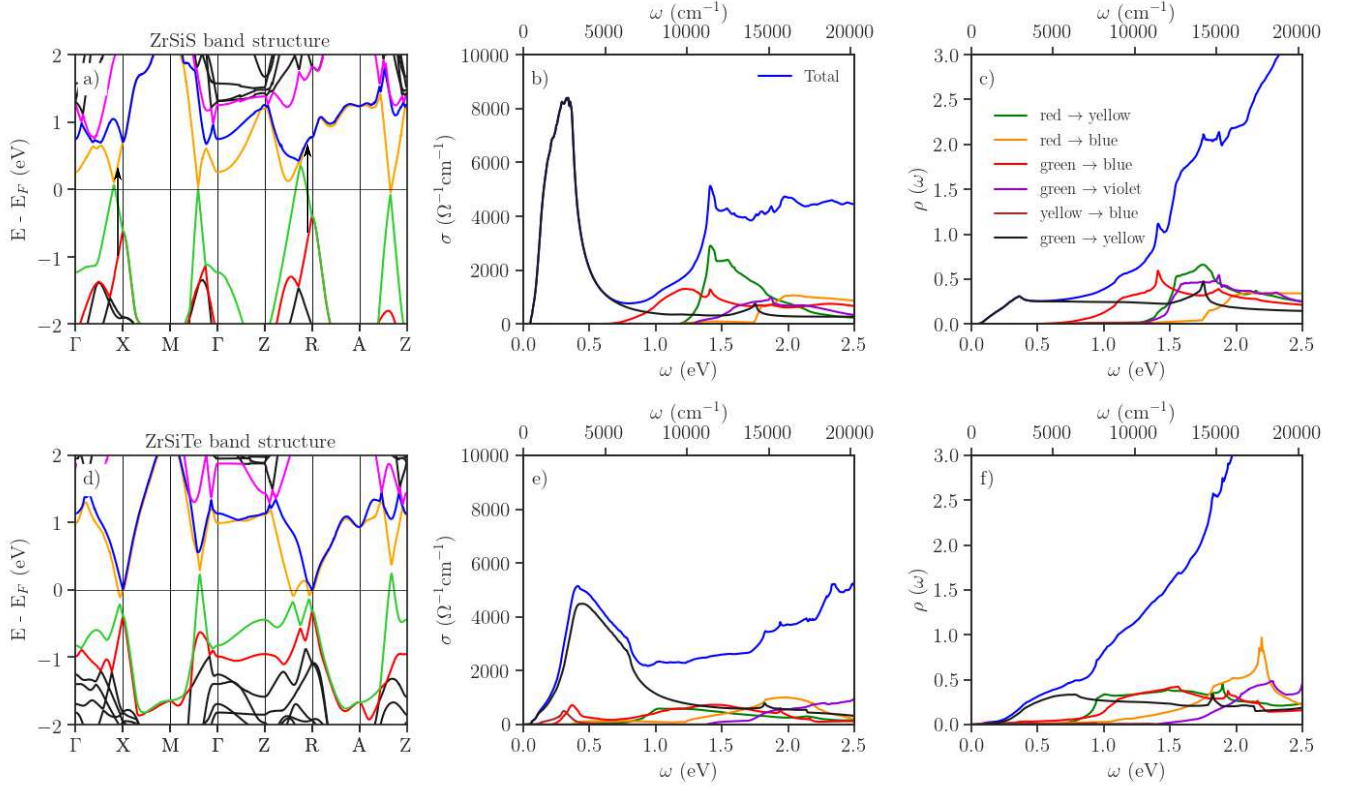


FIG. 4. Calculated band structures of ZrSiS (a) and ZrSiTe (d) with SOC, panels (d, b) and (c, f) show contributions of different band combinations to the optical conductivity  $\sigma$  and joint density of states  $\rho$ , respectively. Black arrows in panel (a) highlight the transitions between almost parallel red and yellow bands in the vicinity of the  $X$  and  $R$  points, which give rise to the L4 peak in the optical conductivity.

the Brillouin zone. The low-frequency boundary correlates with the deviations from this idealized picture due to gapping of the bands or shifting the band crossings away from the Fermi level [27].

The only exception is ZrSiTe. In this compound another pair of bands approaches the Fermi level in the vicinity of the  $X-R$  line [see Fig. 4(d)]. Besides distorting the nodal-line structure in this part of the reciprocal space, the Fermi level is pushed away from the nodal line in the rest of the Brillouin zone. As a result, the optical conductivity spectrum depicted in Fig. 4(e) changes its shape substantially.

## B. Band structure of ZrXY

In order to understand the band structure of the ZrXY compounds, we have constructed a tight-binding model on the basis of Wannier orbitals with Zr  $d$ , Si  $s$ ,  $p$  and S (Te)  $p$  character. In this way, the valence and low-energy conduction band is represented exactly, while the higher-lying conduction bands of Si  $p$  and Zr  $d$  character are disentangled from the rest of the band structure. Next, we have calculated a series of band structures including

an increasing number of hopping processes.

In the first (upper) row of Fig. 5 only the nearest-neighbor Si-Si (in-plane) hopping is taken into account. Even this simple model captures the gross features of the ZrXY band structure, i.e. flat empty Zr- $d$  and occupied S(Te)- $p$  overlaid with broad 2D Si- $sp$  bands. While the Si- $p_z$  bands will be removed from the Fermi level due to the inter-layer hybridization, the crossings of Si- $p_x p_y s$  bands are the precursors of the nodal-line.

In the second row [Figs. 5(c) and (d)], the nearest neighbor Si-Si, Si-Zr and Zr-S(Te) hoppings are included. We note that strong Zr-Si- $p_z$  hybridization removes the  $p_z$  bands from the vicinity of the Fermi level, eventually forming a flat valence band between  $-1$  and  $-2$  eV as well as contributing to the conduction band above 5 eV. The Zr-Si- $p_x p_y s$  hybridization is stronger. A typical shape arising from hybridization between broad and narrow bands can be observed. The band crossing of Si- $p_x p_y s$  bands from the upper row of Fig. 5 are now doubled forming Si-Zr bonding and anti-bonding counterparts below and above the Zr- $d$  manifold. The band structure obtained with unlimited hopping, depicted in Figs. 5(e) and (f), exhibits only quantitative deviations from the one in the second row.

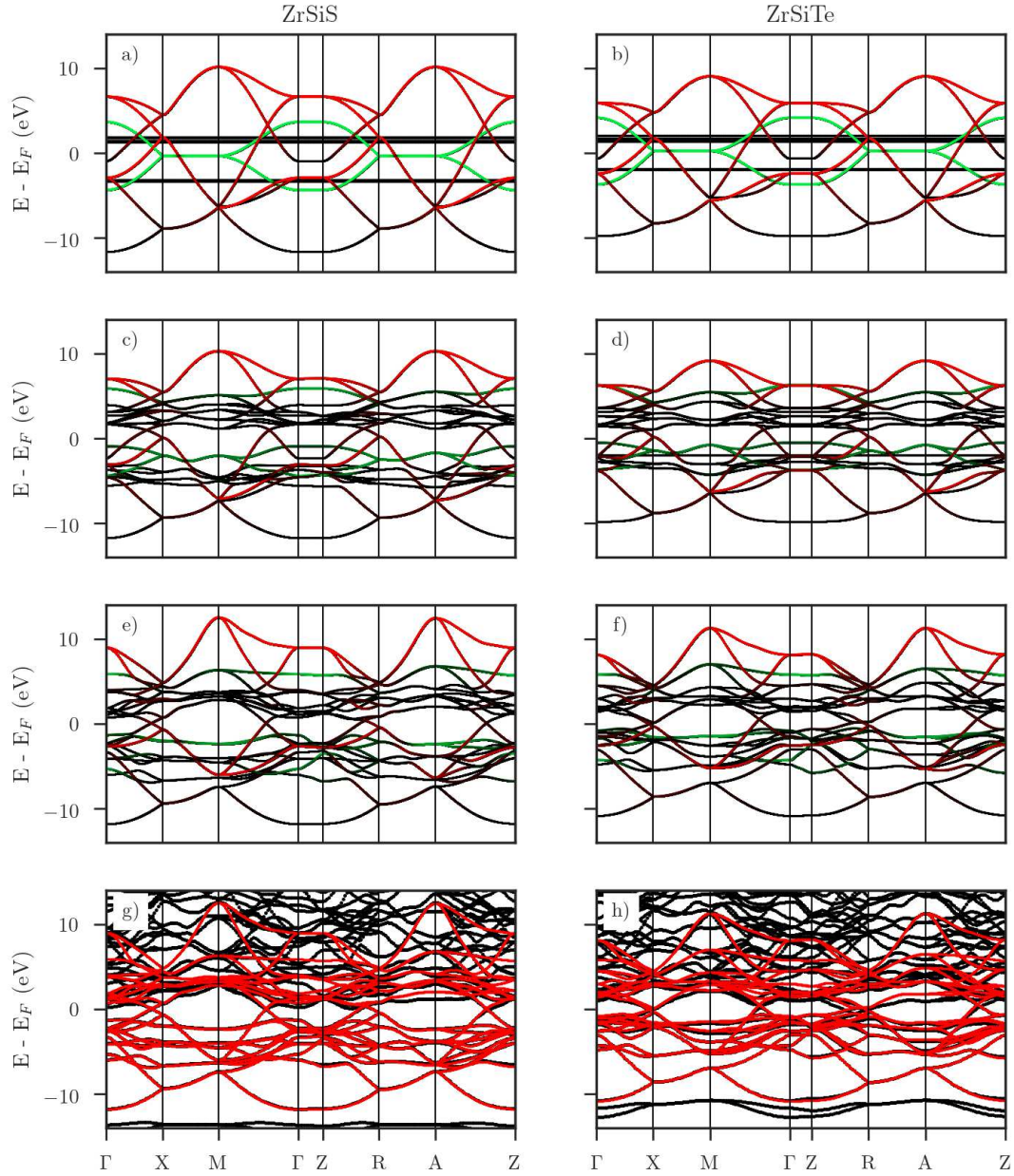


FIG. 5. Wannier band structures of ZrSiS (left) and ZrSiTe (right). Red and green colors in panels (a)-(f) reflect the Si  $pxy$  and Si  $pz$  weights, respectively. The panels (a)-(f) show the band structures obtained for hopping constrained to: nearest neighbors in the Si plane (a)-(b), nearest neighbors Si-Si, Si-Zr and Zr-S/Te (c)-(d) and no constraints (e)-(f). Panels (g,h) show the same Wannier bandstructure (red) as panels (e,f) compared to the full DFT band structures (black).

To summarize, the gross features of the electronic structure of  $\text{ZrXY}$  can be understood as an overlap of broad  $sp$ -bands of a single  $X$  layer overlapping with much narrower  $\text{Zr-}d$  (empty) and  $Y$ - $p$  bands (full). The precursor of the nodal line can be found in the crossing of backfolded  $X$ - $sp_xp_y$  bands. Hybridization with  $\text{Zr}$  layer removes the  $X$ - $p_z$  bands from vicinity of  $E_F$ , while  $X$   $sp_xp_y$ - $\text{Zr}d$  hybrid forms the nodal line.

#### IV. DISCUSSION

Angle-resolved photoemission experiments on  $\text{ZrSiS}$  combined with electronic band structure calculations found a diamond-shaped 3D-like Fermi surface due to a line of Dirac nodes [4, 5]. Furthermore, it was suggested that the electronic band structure of  $\text{ZrSiS}$  contains additional Dirac-like band crossings located several hundred meV above and below  $E_F$  at the  $X$  and  $R$  point of the Brillouin zone. These band crossings are protected by non-symmorphic symmetry against gapping due to the spin-orbit coupling. A comparative study on  $\text{ZrSiS}$ ,  $\text{ZrSiSe}$ , and  $\text{ZrSiTe}$  proposed that the energy positions of these band crossings depend on the  $c/a$  ratio [5, 6, 28], which may serve as a measure for the interlayer bonding [11]. While in  $\text{ZrSiS}$  the band crossings are located at 0.5 - 0.7 eV above and below  $E_F$ , for layered  $\text{ZrSiTe}$  without significant interlayer bonding they are located close to  $E_F$  [6], i.e., with increasing  $c/a$  ratio the band crossings shift towards  $E_F$ . It was also suggested that the electronic structure is very similar for the compounds  $\text{ZrXY}$  ( $X=\text{Si, Ge}$ ;  $Y=\text{S, Se, Te}$ ) including  $\text{ZrSiTe}$ , with only a fine tuning due to the chemical pressure effect [6, 15].

According to our findings, the qualitative similarities in the electronic structure and optical conductivity only hold for compounds  $\text{ZrXY}$  with a similar chemical pressure (for  $c/a$  ratios close to 2.2 - 2.3). In stark contrast,  $\text{ZrSiTe}$  with a significantly larger  $c/a$  ratio [see Fig. 1(b)] and hence smaller interlayer bonding, behaves distinctly different. In particular, the compounds  $\text{ZrSiS}$ ,  $\text{ZrSiSe}$ ,  $\text{ZrGeS}$ , and  $\text{ZrGeTe}$  all show the sharp L4 peak in the optical conductivity, while its energy position depends on the specific compound and presumably on the  $c/a$  ratio. For a quantitative analysis, we fitted the experimental optical conductivity spectra with the Drude-Lorentz model and obtained the energy position of the L4 peak for all studied compounds (see suppl.). In Fig. 6(a) the energy of the L4 peak is plotted as a function of  $c/a$  ratio for  $\text{ZrSiS}$ ,  $\text{ZrSiSe}$ ,  $\text{ZrGeS}$ , and  $\text{ZrGeTe}$ , together with the positions from our theoretical results. We find that with increasing  $c/a$  ratio (decreasing chemical pressure) the sharp L4 peak shifts to lower energies. This holds for  $\text{ZrSiSe}$  as compared to  $\text{ZrSiS}$ , and for  $\text{ZrGeTe}$  as compared to  $\text{ZrGeS}$ . However, when comparing  $\text{ZrSiS}$  with  $\text{ZrGeS}$ , it seems that a simple chemical pressure effect is not strictly given for the replacement of the carbon group element. Apparently, the simple correlation between chemical pressure and peak position does not

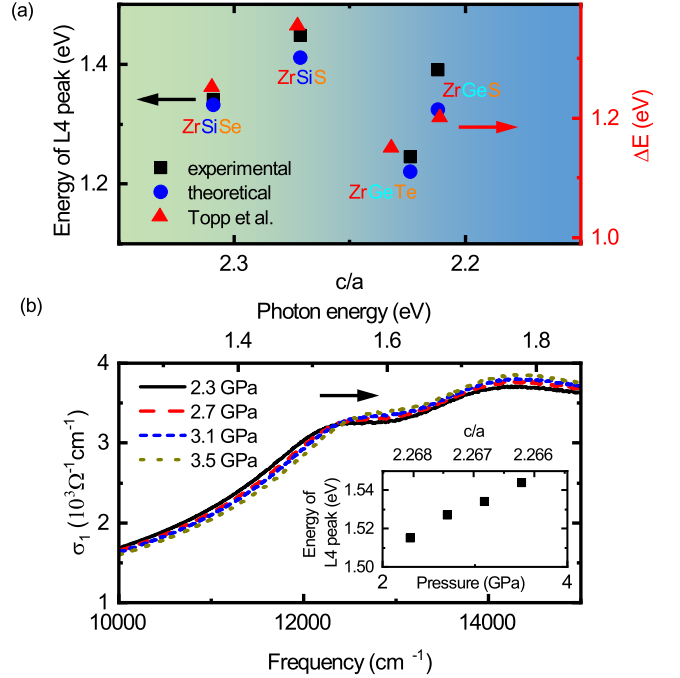


FIG. 6. (a) Energy position of the L4 peak as a function of  $c/a$  ratio, obtained from the experimental and theoretical optical conductivity spectra of  $\text{ZrSiS}$ ,  $\text{ZrSiSe}$ ,  $\text{ZrGeS}$ , and  $\text{ZrGeTe}$ , in comparison with the energy difference  $\Delta E$  between the ungapped band crossings above and below  $E_F$  at the  $X$  point, from Topp et al. [6]. Please note the offset of 0.11 eV between the left and right ordinates. (b) Experimental optical conductivity of  $\text{ZrSiS}$  for selected external pressures in the high-energy range. Inset: Energy position of the L4 peak in  $\text{ZrSiS}$  as a function of external pressure. The pressure dependence of the  $c/a$  ratio was extracted from Ref. [29].

strictly hold for substitutions in the  $X$  square nets. This might be due to the indirect character of the chemical pressure effect induced by the  $X$  substitution, as already described in the introduction.

The L4 peak in the optical conductivity stems from transitions between almost parallel bands in the vicinity of the  $X$  and the  $R$  points of the Brillouin zone, as described above. At the same  $k$  points the ungapped Dirac-like band crossings are located [5, 6]. Therefore, the L4 peak might be related to the band crossings at the  $X$  and  $R$  points, respectively. In order to check this, we compare in Fig. 6(a) the energy difference  $\Delta E$  between the ungapped band crossings above and below  $E_F$  at  $X$ , as obtained by Topp et al. [6], with the energy of the L4 peak from the experimental and theoretical optical conductivity spectra. Apparently, there is a qualitative agreement between the results. The position of the L4 peak in the optical conductivity spectrum may thus serve as a measure for the energy difference between the ungapped band crossings above and below  $E_F$ , which are protected by non-symmorphic symmetry.



The influence of the interlayer bonding on the electronic structure is further corroborated by pressure-dependent optical studies on ZrSiS up to 3.6 GPa. This pressure is below the pressure-induced structural phase transition [29]. Generally, applying hydrostatic pressure to a material is a direct and superior way to tune the dimensionality of a material [30, 31]. For a layered material hydrostatic pressure is expected to mostly affect the lattice parameter along the direction with the highest compressibility (at least for moderate pressures), which is the direction perpendicular to the layers. Hence, under external pressure the distance between the layers is expected to decrease, leading to an increase in the interlayer bonding. According to the optical conductivity of ZrSiS for selected hydrostatic pressures [see Fig. 6(b)], the L4 peak shifts to higher energy with increasing external pressure. This finding is consistent with the observed chemical pressure effect [32].

## V. CONCLUSION

The comparative study of the optical conductivity for the compounds ZrSiY with  $Y=\text{S, Se, Te}$  and ZrGeY with  $Y=\text{S, Te}$  revealed a similar optical conductivity profile, namely a distinct U-shape ending at a sharp peak, for all studied materials except ZrSiTe. The U-shape of the optical conductivity correlates with the nodal-line electronic structure and arises due to strong variation of the dipole matrix elements through the Brillouin zone. This

observation, which agrees with the previous computations of Ref. [14], makes the theoretical models assuming constant matrix elements questionable for this group of materials. The low-frequency boundary of the U-region correlates with the deviations from a flat nodal line. The sharp peak at the high-frequency limit of the U-shaped region has its origin in the transitions between almost parallel bands in the vicinity of the  $X$  and  $R$  points of the Brillouin zone. Its energy position may serve as a measure for the energy difference between the ungapped band crossings above and below  $E_F$  at the  $X$  and  $R$  points. The energy position of the peak significantly depends on the interlayer bonding of the system correlated with the  $c/a$  ratio, which can be tuned by chemical and external pressure. For ZrSiTe with the largest  $c/a$  ratio the optical conductivity profile is very different due to another pair of crossing bands in the vicinity of  $E_F$ , corrugating the nodal-line electronic structure.

## ACKNOWLEDGMENTS

C.K. acknowledges financial support by the Deutsche Forschungsgemeinschaft (DFG), Germany, through grant no. KU 1432/13-1. This work was supported by the ERC Grant Agreement No. 646807 under EU Horizon 2020 (J.F.A., J.K.). The sample synthesis and characterization effort was supported by the US Department of Energy under grant de-sc0019068.

- 
- [1] C. Lee, X. Wei, J. W. Kysar, and J. Hone, *Science* **321**, 385 (2008).
  - [2] K. I. Bolotin, K. J. Sikes, Z. Jiang, M. Klima, G. Fudenberg, J. Hone, P. Kim, and H. L. Stormer, *Solid State Communications* **146**, 351 (2008).
  - [3] A. A. Balandin, S. Ghosh, W. Bao, I. Calizo, D. Teweldebrhan, F. Miao, and C. N. Lau, *Nano Letters* **8**, 902 (2008).
  - [4] M. Neupane, I. Belopolski, M. M. Hosen, D. S. Sanchez, R. Sankar, M. Szlowska, S.-Y. Xu, K. Dimitri, N. Dhakal, P. Maldonado, P. M. Oppeneer, D. Kaczorowski, F. Chou, M. Z. Hasan, and T. Durakiewicz, *Phys. Rev. B* **93**, 201104(R) (2016).
  - [5] L. M. Schoop, M. N. Ali, C. Strasser, A. Topp, A. Varykhalov, D. Marchenko, V. Duppel, S. S. P. Parkin, B. V. Lotsch, and C. R. Ast, *Nat. Commun.* **7**, 11696 (2016).
  - [6] A. Topp, J. M. Lippmann, A. Varykhalov, V. Duppel, B. V. Lotsch, C. R. Ast, and L. M. Schoop, *New J. Phys.* **18**, 125014 (2016).
  - [7] Y.-Y. Lv, B.-B. Zhang, X. Li, S.-H. Yao, Y. B. Chen, J. Zhou, S.-T. Zhang, M.-H. Lu, and Y.-F. Chen, *Appl. Phys. Lett.* **108**, 244101 (2016).
  - [8] R. Sankar, G. Peramaiyan, I. P. Muthuselvam, C. J. Butler, K. Dimitri, M. Neupane, G. N. Rao, M.-T. Lin, and F. C. Chou, *Sci. Rep.* **7**, 40603 (2017).
  - [9] J. Hu, Z. Tang, J. Liu, Y. Zhu, J. Wei, and Z. Mao, *Phys. Rev. B* **96**, 045127 (2017).
  - [10] S. Pezzini, M. R. van Delft, L. M. Schoop, B. V. Lotsch, A. Carrington, M. I. Katsnelson, N. E. Hussey, and S. Wiedmann, *Nature Physics* **14**, 178 (2017).
  - [11] C. Wang and T. Hughbanks, *Inorg. Chem.* **34**, 5524 (1995).
  - [12] S. Klemenz, S. Lei, and L. M. Schoop, arXiv:1808.06619.
  - [13] M. B. Schilling, L. M. Schoop, B. V. Lotsch, M. Dressel, and A. V. Pronin, *Phys. Rev. Lett.* **119**, 187401 (2017).
  - [14] T. Habe and M. Koshino, *Phys. Rev. B* **98**, 125201 (2018).
  - [15] J. Hu, Z. Tang, J. Liu, X. Liu, Y. Zhu, D. Graf, K. Myhro, S. Tran, C. N. Lau, J. Wei, and Z. Mao, *Phys. Rev. Lett.* **117**, 016602 (2016).
  - [16] J. Hu, Y. L. Zhu, D. Graf, Z. J. Tang, J. Y. Liu, and Z. Q. Mao, *Phys. Rev. B* **95**, 205134 (2017).
  - [17] D. B. Tanner, *Phys. Rev. B* **91**, 035123 (2015).
  - [18] M. I. Eremets and Y. A. Timofeev, *Rev. Sci. Instrum.* **63**, 3123 (1992).
  - [19] A. Pashkin, M. Dressel, and C. A. Kuntscher, *Phys. Rev. B* **74**, 165118 (2006).
  - [20] K. P. Blaha, Schwarz, G. K. H. Madsen, D. Kvasnicka, and J. Luitz, "Wien2k, an augmented plane wave + local orbitals program for calculating crystal properties," (2001).
  - [21] Arash A. Mostofi, Jonathan R. Yates, Giovanni Pizzi, Young-Su Lee, Ivo Souza, David Vanderbilt, and Nicola



- Marzari, “An updated version of wannier90: A tool for obtaining maximally-localised wannier functions,” *Computer Physics Communications* **185**, 2309 – 2310 (2014).
- [22] Jan Kune, Ryotaro Arita, Philipp Wissgott, Alessandro Toschi, Hiroaki Ikeda, and Karsten Held, “Wien2wannier: From linearized augmented plane waves to maximally localized wannier functions,” *Computer Physics Communications* **181**, 1888 – 1895 (2010).
- [23] R. Singha, A. K. Pariari, B. Satpati, and P. Mandal, *PNAS* **114**, 2468 (2017).
- [24] J. P. Carbotte, *J. Phys.: Condens. Matter* **29**, 045301 (2017).
- [25] S. P. Mukherjee and J. P. Carbotte, *Phys. Rev. B* **95**, 214203 (2017).
- [26] S. Ahn, E. J. Mele, and H. Min, *Phys. Rev. Lett.* **119**, 147402 (2017).
- [27] Accordingly, ZrGeS is closest to the ideal nodal line system, since its low-frequency limit of the U-shaped optical conductivity is the lowest among the studied compounds. It is interesting to note that ZrGeS has the lowest  $c/a$  ratio among the studied ZrXY materials.
- [28] M. M. Hosen, K. Dimitri, I. Belopolski, P. Maldonado, R. Sankar, N. Dhakal, G. Dhakal, T. Cole, P. M. Oppeneer, D. Kaczorowski, F. Chou, M. Z. Hasan, T. Durakiewicz, and M. Neupane, *Phys. Rev. B* **95**, 161101(R) (2017).
- [29] R. Singha, S. Samanta, S. Chatterjee, A. Pariari, D. Majumdar, B. Satpati, L. Wang, A. Singha, and P. Mandal, *Phys. Rev. B* **97**, 094112 (2018).
- [30] T. Nagata, M. Uehara, J. Goto, J. Akimitsu, N. Motoyama, H. Eisaki, S. Uchida, H. Takahashi, T. Nakanishi, and N. Mori, *Phys. Rev. Lett.* **81**, 1090 (1998).
- [31] A. Pashkin, M. Dressel, M. Hanfland, and C. A. Kuntscher, *Phys. Rev. B* **81**, 125109 (2010).
- [32] Please note that according to Ref. 29 the effect of external pressure on the  $c/a$  ratio in ZrSiS is much smaller than the corresponding effect of chemical pressure. Therefore, the effect of external pressure on the energy position of the L4 peak occurs on a much smaller energy scale as compared to the chemical pressure effect shown in Fig. 6(a).